

Supplementary Information: Simulating Open Quantum System Dynamics on NISQ Computers with Generalized Quantum Master Equations

Yuchen Wang¹, Ellen Mulvihill², Zixuan Hu¹, Ningyi Lyu², Saurabh Shivpuje¹, Yudan Liu³, Micheline B. Soley^{2,4}, Eitan Geva^{*3}, Victor S. Batista^{†2}, and Sabre Kais^{‡1}

¹Department of Chemistry, Department of Physics and Purdue Quantum Science and Engineering Institute, Purdue University, West Lafayette, Indiana 47907, USA

²Department of Chemistry, Yale Quantum Institute, Yale University, New Haven, CT 06511, USA

³Department of Chemistry, University of Michigan, Ann Arbor, MI 48109, USA

⁴Department of Chemistry, Department of Physics, University of Wisconsin-Madison, Madison, WI 53706, USA

May 10, 2023

1 Quantum circuit examples

In this section, we include further details concerning the quantum algorithm, including the dilation process, circuit transpiling, QASM simulations, and simulations running on the IBM quantum computers **ibmq quito** and **ibmq lima**. The normalized time evolution operator of the electronic reduced density operator $\mathcal{G}'(t) = \mathcal{G}(t)/n_c$ (where $\mathcal{G}(t)$ is generated from the GQME formalism) is dilated into a unitary operator $\mathcal{U}_{\mathcal{G}'}(t)$. We start with \mathcal{G}_3 , which corresponds to the $\mathcal{G}(t)$ of the 1500th time step from model 3, and \mathcal{G}_4 , which corresponds to the $\mathcal{G}(t)$ of the 1500th time step from model 4. The matrix of \mathcal{G}_3 and \mathcal{G}_4 are,

*eitan@umich.edu

†victor.batista@yale.edu

‡kais@purdue.edu

respectively:

$$\mathcal{G}_3 = \begin{pmatrix} \circ & & & & \\ \oplus & 0.38 - 3.76 \times 10^{-10}j & 0.04 + 2.90 \times 10^{-2}j & 0.04 - 2.90 \times 10^{-2}j & 0.06 - 1.88 \times 10^{-10}j \\ \oplus & -0.13 + 7.04 \times 10^{-2}j & 0.28 - 2.63 \times 10^{-2}j & 0.02 + 2.37 \times 10^{-2}j & -0.15 - 3.06 \times 10^{-2}j \\ \oplus & -0.13 - 7.04 \times 10^{-2}j & 0.02 - 2.37 \times 10^{-2}j & 0.28 + 2.63 \times 10^{-2}j & -0.15 + 3.06 \times 10^{-2}j \\ \oplus & 0.62 + 3.77 \times 10^{-10}j & -0.04 - 2.90 \times 10^{-2}j & -0.04 + 2.90 \times 10^{-2}j & 0.94 + 1.87 \times 10^{-10}j \end{pmatrix}, \quad (1.1)$$

and

$$\mathcal{G}_4 = \begin{pmatrix} \circ & & & & \\ \oplus & 0.54 + 4.7 \times 10^{-11}j & -1.7 \times 10^{-6} + 5.7 \times 10^{-2}j & -1.6 \times 10^{-6} - 5.6 \times 10^{-2}j & 0.46 + 7.1 \times 10^{-11}j \\ \oplus & -0.46 + 5.7 \times 10^{-2}j & 3.6 \times 10^{-2} + 6.1 \times 10^{-5}j & -1.6 \times 10^{-2} - 5.7 \times 10^{-5}j & -0.46 - 5.7 \times 10^{-2}j \\ \oplus & -0.46 - 5.7 \times 10^{-2}j & -1.6 \times 10^{-2} + 5.7 \times 10^{-5}j & 3.7 \times 10^{-2} - 6.1 \times 10^{-5}j & -0.46 + 5.7 \times 10^{-2}j \\ \oplus & 0.54 - 4.7 \times 10^{-11}j & 1.6 \times 10^{-6} - 5.6 \times 10^{-2}j & 1.6 \times 10^{-6} + 5.6 \times 10^{-2}j & 0.54 - 7.1 \times 10^{-11}j \end{pmatrix}. \quad (1.2)$$

The normalization factors used for model 3 and model 4 are $n_{c3} = 1.376$ and $n_{c4} = 1.376$.

Following the 1-dilation process, the $4 \times 4 \mathcal{G}'(t)$ [derived from corresponding $\mathcal{G}(t)$ divided by the n_c factor] is converted into a unitary $8 \times 8 \mathcal{U}_{\mathcal{G}'(t)}$. We show $\mathcal{U}_{\mathcal{G}'_3}$ and $\mathcal{U}_{\mathcal{G}'_4}$ in the form of heat maps in Fig. S1.

The unitary operation $\mathcal{U}_{\mathcal{G}'(t)}$ is transpiled into a 3-qubit quantum circuit composed of three elementary quantum gates: R_Z , \sqrt{X} , and CX , which have the matrix form:

$$R_Z(\lambda) = \exp \left[-i \frac{\lambda}{2} Z \right] = \begin{pmatrix} e^{-i\lambda/2} & 0 \\ 0 & e^{i\lambda/2} \end{pmatrix} \quad (1.3)$$

$$\sqrt{X} = \frac{1}{2} \begin{pmatrix} 1+i & 1-i \\ 1-i & 1+i \end{pmatrix} \quad (1.4)$$

$$CX_{q_0, q_1} = I \otimes |0\rangle\langle 0| + X \otimes |1\rangle\langle 1| = \begin{pmatrix} \circ & & & & \\ \oplus & 1 & 0 & 0 & 0 \\ \oplus & 0 & 0 & 0 & 1 \\ \oplus & 0 & 0 & 1 & 0 \\ \oplus & 0 & 1 & 0 & 0 \end{pmatrix} \quad (1.5)$$

The full quantum circuits for $\mathcal{U}_{\mathcal{G}'_3}$ and $\mathcal{U}_{\mathcal{G}'_4}$ are shown in Fig. S3 and S4. The probability distribution of the projection measurement results of the two circuits are shown in Fig. S2. Both the QASM simulator results and the real machine simulated results are recorded.

2 Amplitude-damping model

In this section, we will show that the method of flattening the density matrix for dilation, which was outlined in the supplementary information in our previous publication [1], can be implemented on the quantum device for the simple amplitude damping model. The same method is verified by the implementation described in this and the following section. This verification allows us to confidently incorporate the general algorithm with GQME.

The general algorithm for open quantum system dynamics is applicable to the time-evolution of density matrices governed by Kraus operators [1]. The time-evolution representation for such open systems is given by $\hat{\rho}(t) =$

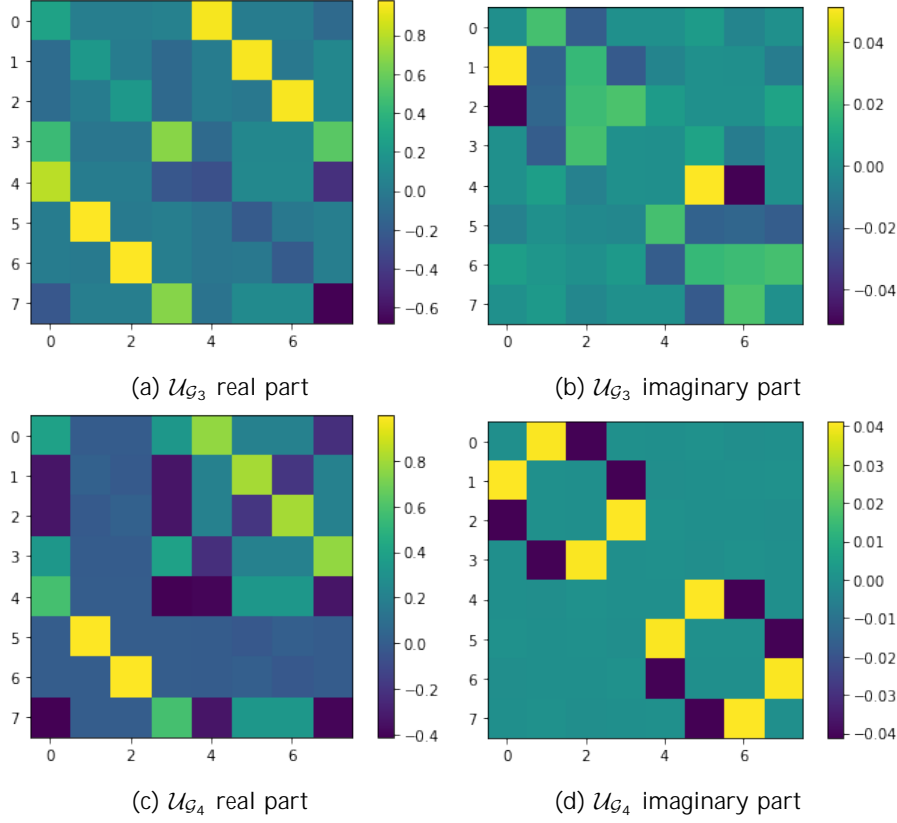


Figure S1: Heat map illustrations of the dilated 8×8 unitary matrix $\mathcal{U}_{\mathcal{G}_3}$ and $\mathcal{U}_{\mathcal{G}_4}$ for the 1500th $\mathcal{G}(t)$ matrix, \mathcal{G}_3 at $t = 2.25\Gamma^{-1}$ for model 3 with (a) the real part of the matrix and (b) the imaginary part of the matrix and \mathcal{G}_4 at $t = 6.75\Gamma^{-1}$ for model 4 with (c) the real part of the matrix and (d) the imaginary part of the matrix.

$\mathbb{P}_k \mathcal{M}_k(t) \hat{\rho} \mathcal{M}_k^\dagger(t)$. For simplicity, the notation of time dependency is omitted hereafter for superoperators \mathcal{M} and superoperators derived from it. In the first step, the density matrix is flattened to vector form: $\hat{\rho} \rightarrow \mathbf{v}_\rho = (\rho_{11}, \dots, \rho_{1n}, \rho_{21}, \dots, \rho_{2n}, \dots, \rho_{n1}, \dots, \rho_{nn})^T$. We calculate the Frobenius norm of \mathbf{v}_ρ as $\|\mathbf{v}_\rho\|_F = \sqrt{\sum_{ij} |\rho_{ij}|^2}$ and divide \mathbf{v}_ρ by $\|\mathbf{v}_\rho\|_F$ to normalize \mathbf{v}_ρ . Next,

for every k , the \mathcal{M}_k is transformed into $\tilde{\mathcal{M}}_k = \mathcal{M}_k \otimes I$; similarly, the \mathcal{M}_k^\dagger is transformed into $\tilde{\mathcal{N}}_k = I \otimes \bar{\mathcal{M}}_k$. The \otimes stands for the Kronecker product and the bar over \mathcal{M}_k indicates complex conjugation. The new equivalent form for

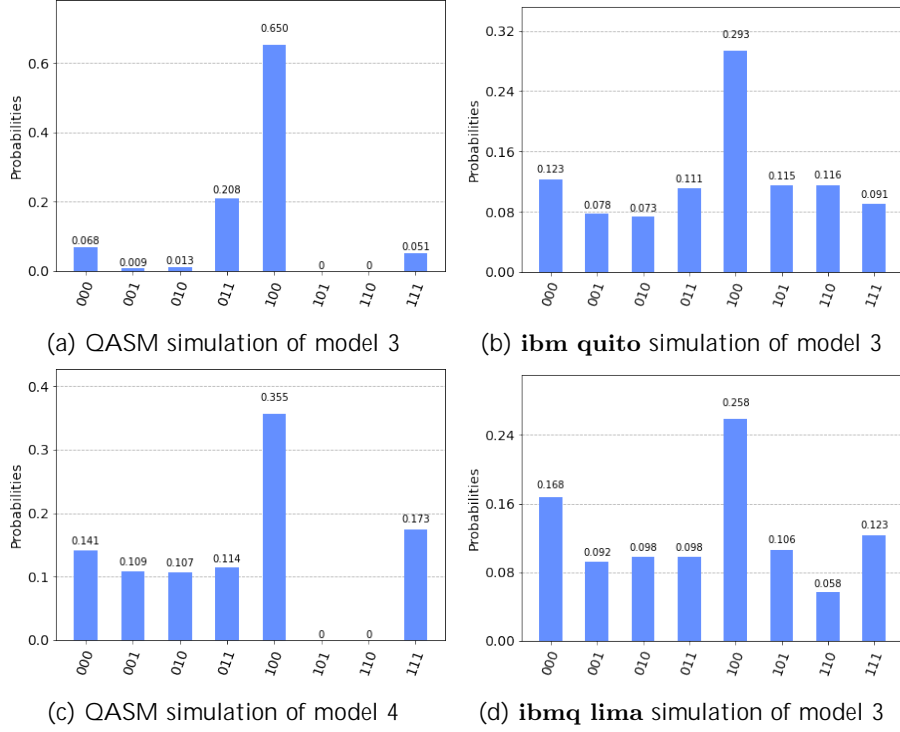


Figure S2: Probability distribution of the quantum state after the projection measurement applied to the circuit for \mathcal{U}_{G_3} on (a) the QASM and (b) **ibm quito** quantum computer and \mathcal{U}_{G_4} on (c) the QASM and (d) **ibmq lima** quantum computer. The $|000\rangle$ state corresponds to the population squared of the donor state $\sigma_{DD}(t)$ and the $|100\rangle$ state corresponds to the population squared of the acceptor state $\sigma_{AA}(t)$. The last four states are ancilla states.

the Kraus representation is:

$$\mathcal{M}_k \hat{\rho} \mathcal{M}_k^\dagger \overset{\text{equivalent}}{\longleftrightarrow} \tilde{\mathcal{N}}_k \tilde{\mathcal{M}}_k \mathbf{v}_\rho. \quad (2.1)$$

The input state is initialized to the normalized \mathbf{v}_ρ in the execution. In Ref. 1, it is shown that the Kraus operator \mathcal{M}_k is a contraction. Therefore $\tilde{\mathcal{M}}_k = \mathcal{M}_k \otimes I$ and $\tilde{\mathcal{N}}_k = I \otimes \tilde{\mathcal{M}}_k$ are also contractions as per the norm property of the Kronecker product. To build the quantum circuit of $\tilde{\mathcal{N}}_k \tilde{\mathcal{M}}_k \mathbf{v}_\rho$ with unitary gates, we need two separate 2-dilations:

$$\tilde{\mathcal{N}}_k \tilde{\mathcal{M}}_k \mathbf{v}_\rho \xrightarrow{\text{unitary dilation}} \mathcal{U}_{\tilde{\mathcal{N}}_k} \mathcal{U}_{\tilde{\mathcal{M}}_k} \mathbf{v}_\rho^T, 0, \dots, 0^T. \quad (2.2)$$

For \mathcal{M}_k of dimension $n \times n$, $\tilde{\mathcal{M}}_k$ and $\tilde{\mathcal{N}}_k$ are $n^2 \times n^2$; and consequently, the 2-dilations $\mathcal{U}_{\tilde{\mathcal{M}}_k}$ and $\mathcal{U}_{\tilde{\mathcal{N}}_k}$ are $3n^2 \times 3n^2$. The $\mathcal{U}_{\tilde{\mathcal{M}}_k}$ and $\mathcal{U}_{\tilde{\mathcal{N}}_k}$ are fragmented into sequences of two-level unitary gates and tallied to compute the gate complexity.

To realize $\tilde{\mathcal{N}}_k \tilde{\mathcal{M}}_k \mathbf{v}_\rho$, the total gate complexity is $3n^3 + n^2$ for each k . The classical complexity to realize $\mathcal{M}_k \hat{\rho} \mathcal{M}_k^\dagger$ based on a naive algorithm is higher, though of same order as quantum algorithm, namely $4n^3 - 2n^2$.

All the evolved density matrices in the circuit calculated at each timestep are obtained as the output vector $\mathbf{v}_k(t) = \tilde{\mathcal{N}}_k \tilde{\mathcal{M}}_k \mathbf{v}_\rho$. The desired information to be collected from the density matrix is extracted by applying projection measurements on $\mathbf{v}_k(t)$ using an optical setup [2]. The detailed procedure for obtaining information located at both diagonal and off-diagonal elements of $\hat{\rho}_k(t)$ from final $\mathbf{v}_k(t)$ is described in the supplementary information of Ref. 1.

3 Simulation of the amplitude damping model with Kraus operators

We tested the theory mentioned in the previous section for spontaneous emission of a 2-level atom modeled by amplitude-channel damping. The corresponding Lindblad master equation is:

$$\dot{\hat{\rho}}(t) = \gamma \sigma^+ \hat{\rho}(t) \sigma^- - \frac{1}{2} \{ \sigma^- \sigma^+, \hat{\rho}(t) \} ,$$

where the spontaneous emission rate is $\gamma = 1.52 \times 10^9 \text{ s}^{-1}$, and the $\sigma^+ = |0\rangle\langle 1|$ and $\sigma^- = (\sigma^+)^\dagger$ are Pauli raising and lowering operators, respectively. The density matrix $\rho(t)$ in the Kraus representation is as follows:

$$\begin{aligned} \hat{\rho}(t) &= \mathcal{M}_0(t) \hat{\rho} \mathcal{M}_0(t)^\dagger + \mathcal{M}_1(t) \hat{\rho} \mathcal{M}_1(t)^\dagger, \\ \mathcal{M}_0(t) &= \frac{1+\sqrt{e^{-\gamma t}}}{2} \mathbf{I} + \frac{1-\sqrt{e^{-\gamma t}}}{2} \sigma_z = \begin{pmatrix} 1 & 0 \\ 0 & \sqrt{e^{-\gamma t}} \end{pmatrix}, \\ \mathcal{M}_1(t) &= \sqrt{1-e^{-\gamma t}} \sigma^+ = \begin{pmatrix} 0 & \sqrt{1-e^{-\gamma t}} \\ 0 & 0 \end{pmatrix}. \end{aligned} \quad (3.1)$$

For \mathcal{M}_k of dimension 2×2 , $\tilde{\mathcal{M}}_k$, $\tilde{\mathcal{N}}_k$, and \mathcal{D}_A are 4×4 matrices, as given below in Eq. (3.2). In this way, the 2-dilations $\mathcal{U}_{\mathcal{M}_k}$ and $\mathcal{U}_{\tilde{\mathcal{M}}_k}$ are 12×12 following the k -dilation [1,3]. Note that, though these superoperators are time dependent, only for simplicity we omitted the notation of time dependency. However, realization of the dilated matrices using quantum gate is of dimension of form $2^n \times 2^n$. We append the dilated matrix with an ancillary 12×4 zero matrix on the right and 4×12 at the bottom, and an 4×4 identity matrix along the diagonal. The resulting dilated superoperator matrix is 16×16 , requiring 4 qubits for quantum implementation. Quantum implementation is accomplished with Qiskit as mentioned in the main text.

$$\begin{aligned}
\tilde{\mathcal{M}}_0 &= \begin{array}{c} \textcircled{1} \\ \textcircled{0} \\ \textcircled{0} \\ \textcircled{0} \\ \textcircled{0} \end{array} \begin{array}{cccc} 0 & 0 & 0 & 1 \\ 1 & 0 & 0 & 0 \\ 0 & \sqrt{e^{-\gamma t}} & 0 & 0 \\ 0 & 0 & \sqrt{e^{-\gamma t}} & 0 \end{array} \begin{array}{c} \textcircled{1} \\ \textcircled{C} \\ \textcircled{A} \end{array}, \quad \tilde{\mathcal{N}}_0 = \begin{array}{c} \textcircled{1} \\ \textcircled{0} \\ \textcircled{0} \\ \textcircled{0} \\ \textcircled{0} \end{array} \begin{array}{cccc} 0 & 0 & 0 & 1 \\ \sqrt{e^{-\gamma t}} & 0 & 0 & 0 \\ 0 & 1 & 0 & 0 \\ 0 & 0 & 0 & \sqrt{e^{-\gamma t}} \end{array} \begin{array}{c} \textcircled{1} \\ \textcircled{C} \\ \textcircled{A} \end{array}, \\
\mathcal{D}_{\tilde{\mathcal{M}}_0} &= \begin{array}{c} \textcircled{0} \\ \textcircled{0} \\ \textcircled{0} \\ \textcircled{0} \\ \textcircled{0} \end{array} \begin{array}{cccc} 0 & 0 & 0 & 1 \\ 0 & 0 & 0 & 0 \\ 0 & \sqrt{1-e^{-\gamma t}} & 0 & 0 \\ 0 & 0 & \sqrt{1-e^{-\gamma t}} & 0 \end{array} \begin{array}{c} \textcircled{1} \\ \textcircled{C} \\ \textcircled{A} \end{array}, \quad \mathcal{D}_{\tilde{\mathcal{N}}_0} = \begin{array}{c} \textcircled{0} \\ \textcircled{0} \\ \textcircled{0} \\ \textcircled{0} \\ \textcircled{0} \end{array} \begin{array}{cccc} 0 & 0 & 0 & 1 \\ \sqrt{1-e^{-\gamma t}} & 0 & 0 & 0 \\ 0 & 0 & 0 & 0 \\ 0 & 0 & 0 & \sqrt{1-e^{-\gamma t}} \end{array} \begin{array}{c} \textcircled{1} \\ \textcircled{C} \\ \textcircled{A} \end{array}, \\
\tilde{\mathcal{M}}_1 &= \begin{array}{c} \textcircled{0} \\ \textcircled{0} \\ \textcircled{0} \\ \textcircled{0} \\ \textcircled{0} \end{array} \begin{array}{cccc} 0 & 0 & 0 & 1 \\ \sqrt{1-e^{-\gamma t}} & 0 & 0 & 0 \\ 0 & 0 & \sqrt{1-e^{-\gamma t}} & 0 \\ 0 & 0 & 0 & 0 \end{array} \begin{array}{c} \textcircled{1} \\ \textcircled{C} \\ \textcircled{A} \end{array}, \quad \tilde{\mathcal{N}}_1 = \begin{array}{c} \textcircled{0} \\ \textcircled{0} \\ \textcircled{0} \\ \textcircled{0} \\ \textcircled{0} \end{array} \begin{array}{cccc} \sqrt{1-e^{-\gamma t}} & 0 & 0 & 1 \\ 0 & 0 & 0 & 0 \\ 0 & 0 & 0 & \sqrt{1-e^{-\gamma t}} \\ 0 & 0 & 0 & 0 \end{array} \begin{array}{c} \textcircled{1} \\ \textcircled{C} \\ \textcircled{A} \end{array}, \\
\mathcal{D}_{\tilde{\mathcal{M}}_1} &= \begin{array}{c} \textcircled{1} \\ \textcircled{0} \\ \textcircled{0} \\ \textcircled{0} \\ \textcircled{0} \end{array} \begin{array}{cccc} 0 & 0 & 0 & 1 \\ 1 & 0 & 0 & 0 \\ 0 & \sqrt{e^{-\gamma t}} & 0 & 0 \\ 0 & 0 & \sqrt{e^{-\gamma t}} & 0 \end{array} \begin{array}{c} \textcircled{1} \\ \textcircled{C} \\ \textcircled{A} \end{array}, \quad \mathcal{D}_{\tilde{\mathcal{N}}_1} = \begin{array}{c} \textcircled{1} \\ \textcircled{0} \\ \textcircled{0} \\ \textcircled{0} \\ \textcircled{0} \end{array} \begin{array}{cccc} 0 & 0 & 0 & 1 \\ \sqrt{e^{-\gamma t}} & 0 & 0 & 0 \\ 0 & 1 & 0 & 0 \\ 0 & 0 & 0 & \sqrt{e^{-\gamma t}} \end{array} \begin{array}{c} \textcircled{1} \\ \textcircled{C} \\ \textcircled{A} \end{array}.
\end{aligned} \tag{3.2}$$

For an initial density $\hat{\rho}(0) = \frac{1}{4} \begin{array}{c} 1 \\ 1 \\ 1 \\ 3 \end{array}$, we calculate the populations in the basis $\{|0\rangle, |1\rangle\}$ from $t = 0$ to $t = 1000$ ps with a time step of 10 ps. With $\|\hat{\rho}\|_{HS} = \frac{\sqrt{3}}{2}$, the input state is:

$$\mathbf{v}_0 = \frac{1}{\|\hat{\rho}\|_{HS}} \begin{array}{c} \textcircled{1} \\ \textcircled{0} \\ \textcircled{0} \\ \textcircled{0} \\ \textcircled{0} \end{array} \begin{array}{cccc} 1 & 1 & 1 & 3 \\ 0 & 0 & 0 & 0 \\ \dots & \dots & \dots & \dots \\ 0 & 0 & 0 & 0 \end{array} \begin{array}{c} \textcircled{1} \\ \textcircled{C} \\ \textcircled{A} \end{array} = \frac{1}{2\sqrt{3}} \begin{array}{c} \textcircled{1} \\ \textcircled{0} \\ \textcircled{0} \\ \textcircled{0} \\ \textcircled{0} \end{array} \begin{array}{cccc} 1 & 1 & 1 & 3 \\ 0 & 0 & 0 & 0 \\ \dots & \dots & \dots & \dots \\ 0 & 0 & 0 & 0 \end{array} \begin{array}{c} \textcircled{1} \\ \textcircled{C} \\ \textcircled{A} \end{array}, \tag{3.3}$$

where $m = 12$ for the vector \mathbf{v}_ρ^T to be of length 16. After extracting the output $\mathbf{v}_k(t)$, the ground state and excited state populations are obtained as the first and fourth entry of the vector, respectively. The Fig. S5 result manifests the consistency with the result in Ref. 1.

References

- [1] Z. Hu, R. Xia, and S. Kais, “A quantum algorithm for evolving open quantum dynamics on quantum computing devices,” *Sci. Rep.*, vol. 10, no. 1, pp. 1–9, 2020.
- [2] C. Sparrow, E. Martín-López, N. Maraviglia, A. Neville, C. Harrold, J. Carolan, Y. N. Joglekar, T. Hashimoto, N. Matsuda, J. L. O’Brien, D. P. Tew, and A. Laing, “Simulating the vibrational quantum dynamics of molecules using photonics,” *Nature*, vol. 557, no. 7707, pp. 660–667, 2018.

- [3] E. Levy and O. M. Shalit, “Dilation theory in finite dimensions: the possible, the impossible and the unknown,” *Rocky Mt. J. Math.*, vol. 44, no. 1, pp. 203–221, 2014.

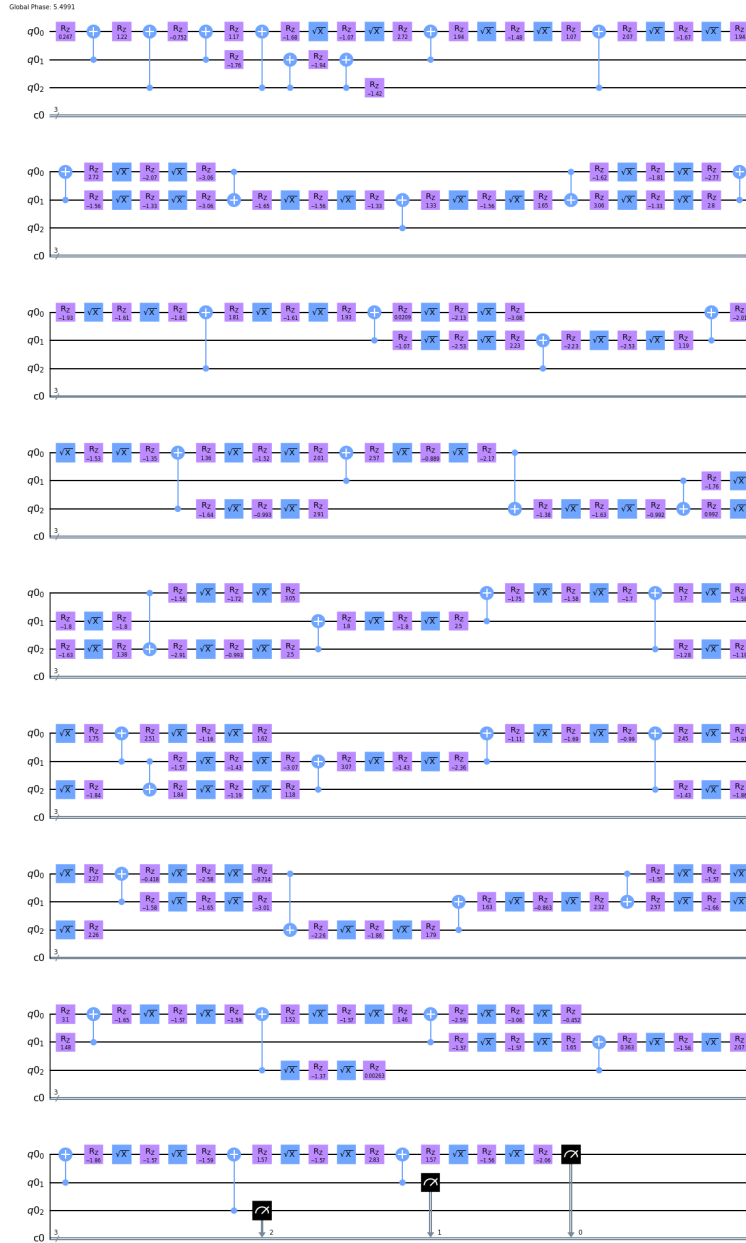


Figure S3: Transpiled quantum circuit of the dilated \mathcal{U}_{G_3} matrix at 1500 time steps for model 3. Each horizontal black line denotes a qubit. The \sqrt{X} gate (blue square) is the square root of X gate; the R_z gate (magenta square) is the rotation Z gate. The two-qubit gates are the controlled-NOT gate, where the dot denotes the controlled qubit and --- denotes the target qubit. The black gates at the end of the circuit denote the projection measurements. The number of required R_z , \sqrt{X} , and CNOT gates are 153, 98, and 41, respectively.

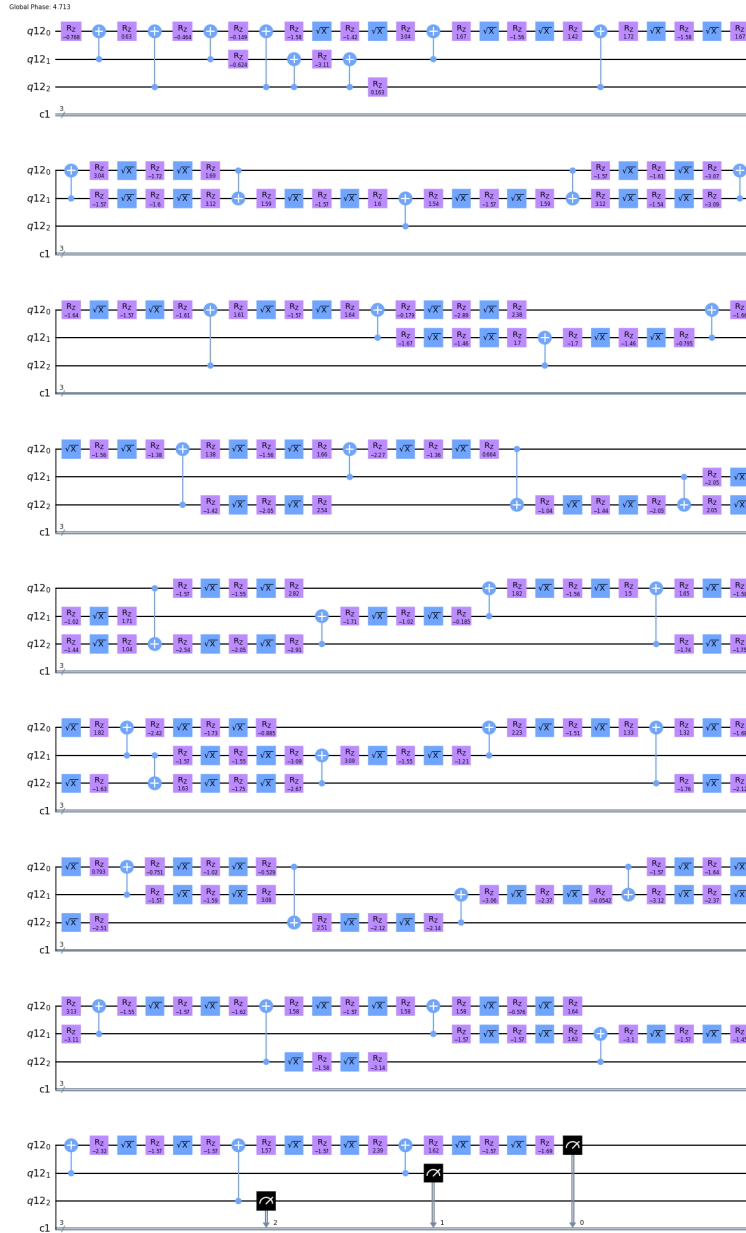


Figure S4: Transpiled quantum circuit of the dilated \mathcal{U}_{G_4} matrix at 1500 time steps for model 4. Each horizontal black line denotes a qubit. The \sqrt{X} gate (blue square) is the square root of X gate; the R_z gate (magenta square) is the rotation Z gate. The two-qubit gates are the controlled-NOT gate, where the dot denotes the controlled qubit and \square denotes the target qubit. The black gates at the end of the circuit denote the projection measurements. The number of required R_z , \sqrt{X} , and CNOT gates are 153, 98, and 41, respectively.

